RSC Advances

PAPER

View Article Online
View Journal | View Issue

Check for updates

Cite this: *RSC Adv.*, 2017, **7**, 29284

Synthesis of mesoporous SiO_2/Cu_2O–graphene nanocomposites and their highly efficient photocatalytic performance for dye pollutants†

Dinh Cung Tien Nguyen,[a] Kwang Yeon Cho[b] and Won-Chun Oh *[a]

A mesoporous SiO_2/Cu_2O–graphene composite, a novel material, was successfully synthesized using a self-assembly method with tetraethyl orthosilicate (TEOS). During the reaction, Cu_2O and silica nanoparticles were loaded on the graphene sheets. The mesoporous structure, morphology, pore diameter, pore volume, and surface area of the mesoporous SiO_2/Cu_2O–graphene composite photocatalysts were obtained *via* X-ray diffraction (XRD), scanning electron microscopy (SEM), energy dispersive X-ray (EDX) analysis, transmission electron microscopy (TEM), Raman spectroscopy, ultraviolet-visible diffuse reflectance spectroscopy (UV-vis DRS), X-ray photoelectron spectroscopy (XPS), FT-IR spectra, nitrogen adsorption/desorption isotherms using the BET and BJH method and photocurrent analyses. The photocatalytic degradation of rhodamine B (RhB), methylene blue trihydrate (MB), and reactive black B (RBB) in an aqueous solution under visible light irradiation was observed *via* UV spectrophotometry after measuring the decrease in their concentrations. The mesoporous structure of silica nanoparticles with a large surface plays a major role in the increased photodegradation as well as in the decomposition by the catalysts. Through recycling experiments, we conclude that the mesoporous SiO_2/Cu_2O–graphene composite had good stability during photocatalysis under visible light irradiation. The mesoporous SiO_2/Cu_2O–graphene nanocomposite is expected to become a candidate material for photodegradation with excellent performance.

Received 28th March 2017
Accepted 31st May 2017

DOI: 10.1039/c7ra03526h

rsc.li/rsc-advances

Open Access Article. Published on 05 June 2017. Downloaded on 9/15/2024 10:19:27 AM.
This article is licensed under a Creative Commons Attribution-NonCommercial 3.0 Unported Licence.

1. Introduction

Graphene has been successfully decorated with numerous inorganic materials such as Au, ZnO, TiO_2, and Cu salts through various methods, leading to nanocomposites with a photocatalytic activity that is useful in the degradation of organic dyes.[1–4] Of these, graphene-based composite materials have attracted a significant amount of attention because recent studies have shown their applicability in electronics, photocatalytic systems, and photovoltaic devices.[5–7] The graphene surface decorated with nanomaterials can overcome the aggregation of individual graphene sheets and of the nanomaterials themselves.[8–10] With the outstanding development of science and technology, some new advances on graphene-based photocatalyst have been presented. Ting Xiong *et al.* demonstrated the important role of reduced graphene oxide (RGO) in UV-induced photocatalysis of RGO-based nanocomposites.[11] Yuhan Li *et al.* proposed enhancing the photocatalytic activity of bulk g-C_3N_4 by introducing mesoporous structures and hybridizing with graphene.[12]

Cu_2O is a p-type semiconductor oxide that is considered to have potential for use in catalytic systems, fuel cells, and solar cells.[13,14] Cu_2O has the advantage of a narrow band gap energy (2.00 eV) and a suitable energy level position that make it a promising inorganic material for use in photodegradation under visible light.[15–17] In addition, Cu_2O is inexpensive and non-toxic, with a high chemical durability that is particularly manifested in its unsurpassed optical decomposition, and as such is a promising candidate for scientists to prepare highly applicable nanocomposites.[18] For example, Chen Kunfeng *et al.* reported on a Cu_2O nanocrystal and Cu_2O–graphene composite paper for use as lithium-ion battery anode materials.[19] Zhang *et al.* synthesized a Cu_2O–graphene using the solvothermal method and also discussed the use of Cu_2O–graphene in an electrochemical sensor for dopamine.[20]

Recently, silica nanoparticles (SiO_2) have become popular materials with potential applications in numerous fields, including ceramics, catalysts, pharmaceutical products, electronic packaging, photonic and chemical–mechanical polishing due to their ordered mesostructure, large surface area, flexible pore size, and thermal stability.[21–23] Due to such advantages, silica nanoparticles (SiO_2) have been considered to have be

[a]*Department of Advanced Materials Science & Engineering, Hanseo University, Seosan, Chungnam, Korea, 356-706. E-mail: wc_oh@hanseo.ac.kr; Fax: +82-41-688-3352; Tel: +82-41-660-1337*

[b]*Korea Institutes of Ceramic Engineering and Technology, Soho-ro, Jinju-Si, Gyeongsangnam-do, Republic of Korea*

† Electronic supplementary information (ESI) available. See DOI: 10.1039/c7ra03526h

This journal is © The Royal Society of Chemistry 2017

Open Access Article. Published on 05 June 2017. Downloaded on 9/15/2024 10:19:27 AM.
This article is licensed under a Creative Commons Attribution-NonCommercial 3.0 Unported Licence.

photocatalyst with higher efficiency than TiO_2.[20,24,25] In addition, the improvement in the pore diameter, pore volume and surface area of the silica nanoparticles has attracted a significant amount of attention in various fields of science. Fengyuan Zhang[20] observed that surfactants will improve the pore size and the distribution of the silica nanoparticles.[26] The combination of graphene oxide and silica nanoparticles exhibits many outstanding properties when compared with bare graphene oxide and silica nanoparticles,[27] and coating silica nanoparticles with many different kinds of inorganic materials has been reported to result in unique properties with many uses.[28,29] With their different band gap energy levels, Cu_2O and SiO_2 particles can be combined to produce a composite with a highly efficient photocatalysis of dye pollutants under visible light irradiation.[30–32] Nevertheless, the synthesis of mesoporous SiO_2/Cu_2O–graphene composites through a facile method, such as the self-assembly method, and their effective use in photocatalytic systems has not been demonstrated yet.

In this study, a mesoporous SiO_2/Cu_2O–graphene composite was prepared using a self-assembly method. A facile route was implemented to synthesize the mesoporous SiO_2/Cu_2O–graphene using tetraethyl orthosilicate (TEOS) as the silica precursor at a pH of 9.5–10. The dispersion medium consisted of a mixture of water and ethanol. Cetyltrimethylammonium bromide (CTAB) was used as the structure creator, and the silica mesoparticles formed after hydrolysis. The structure and morphology of the mesoporous SiO_2/Cu_2O–graphene composites were characterized *via* X-ray diffraction (XRD), scanning electron microscopy (SEM), energy dispersive X-ray (EDX) analysis, transmission electron microscopy (TEM), Raman spectroscopy, ultraviolet-visible diffuse reflectance spectroscopy (UV-vis-DRS), X-ray photoelectron spectroscopy (XPS). The FT-IR spectra were also recorded as evidence to confirm the structure of the survey composites. The pore diameter, pore volume and surface area of the mesoporous SiO_2/Cu_2O–graphene composites were determined *via* nitrogen adsorption/desorption isotherms using the BET and BJH method. Photodegradation experiments were then conducted with rhodamine B (RhB), methylene blue trihydrate (MB), and reactive black B (RBB) organic dyes in an aqueous solution under visible light irradiation. The recycling experiments were carried out for five repeated cycles to investigate the stability of the photocatalysts.

2. Experimental

2.1 Reagents

Graphene oxide was prepared in the laboratory from natural graphite using Hummer–Offerman's method and was used to form the composites. Copper(II) acetate ($Cu(CH_3COO)_2 \cdot H_2O$, 95%), rhodamine B (RhB, $C_{28}H_{31}ClN_2O_3$), and methylene blue trihydrate (MB, $C_{18}H_{18}ClN_3S \cdot 3H_2O$) were purchased from Samchun Pure Chemicals Co. Ltd, Korea. Reactive Black B 195% (RBB) was purchased from JAY Chemical Industries Limited, India. Polyvinylpyrrolidone (PVP) K-30 was purchased from Junsei Chemical Co., Ltd, Japan. Ethanol (C_2H_5OH, 95%) was purchased from Duskan Pure Chemicals Co. Ltd, Korea. Tetraethyl orthosilicate (TEOS, 99%) was purchased from Aldrich Chemistry, Germany. Cetyltrimethylammonium bromide (CTAB, $C_{19}H_{42}BrN$, 99%) and ammonium hydroxide (NH_4OH), and ethylene glycol ($C_2H_6O_2$, 99%) were purchased from Daejung Chemicals Co. Ltd, Korea. Urea ($CO(NH_2)_2$) was purchased from Sinopharm Chemical Reagent Co., Ltd. All chemicals were used without further purification, and all experiments were carried out using distilled water.

2.2 Synthesis nanocomposites

2.2.1 Synthesis of the Cu_2O nanoparticles. 0.32 g $Cu(CH_3COO)_2 \cdot H_2O$ was dissolved in 50 mL distilled water and 8 mL of ethylene glycol, then magnetic stirred for 30 min. Then, 0.24 g $CO(NH_2)_2$ was added into the above solution and keep stirring for 30 min to form a transparent solution. After a hydrothermal reaction occurred at 180 °C for 10 hours, the temperature of the mixture was brought down to ambient temperature, and the mixture was filtered using Whatman filter paper ($\Phi = 110$ mm). The obtained solid was collected and washed with distilled water 3 times and ethanol 95% twice. After drying under vacuum at 70 °C for 3 hours, the obtained samples were collected for characterization.

2.2.2 Synthesis of the Cu_2O–graphene nanocomposite. 0.005 mol $Cu(CH_3COO)_2 \cdot H_2O$ was dissolved in 50 mL distilled water, then heated to 60 °C with magnetic stirring for 30 min to form part A. Sonication of the graphene oxide (0.01 g) in 10 mL of 95% ethanol was conducted for 30 min to form part B. Part A was mixed with part B and 0.1 g PVP, with continued vigorous stirring for 1 hour at 80 °C. The pH value was adjusted with NaOH 1 M until it reached pH 9 and was maintained for 1 hour. After a hydrothermal reaction occurred at 180 °C during 10 hours, graphene oxide was reduced to a graphene nanosheet with the deposition of Cu_2O compounds on the surface to form the Cu_2O–graphene nanocomposite. Afterward, the temperature of the mixture was brought down to ambient temperature, and the mixture was filtered using Whatman filter paper ($\Phi =$ 110 mm). The obtained solid was collected and washed with distilled water 3 times and ethanol 95% twice. The Cu_2O–graphene nanocomposites were obtained after drying in a vacuum at 90 °C for 24 h. After drying under vacuum at 105 °C for 24 h, the achieved powder was calcined at room temperature to 550 °C for 8 hours followed by heating at 550 °C for 6 hours.

2.2.3 Synthesis mesoporous SiO_2/Cu_2O–graphene nanocomposite. 0.36 g CTAB was dissolved in 57 mL distilled water, then stirred with magnetic stirring for 30 min to form part C. Part D was obtained *via* ultrasonication of the Cu_2O–graphene nanocomposite (0.4 g) in 20 mL distilled water for 30 min. Separately, 4 mL TEOS, 80 mL ethanol, and 5 mL NH_3 25% were mixed under vigorous stirring to form part E. Part C, D, and E were mixed together with continued vigorous stirring for 6 hours at room temperature. Eventually, the pH value was adjusted with NH_4OH 25% until reaching pH 9.5–10 and was then maintained for 1 hour. The above dispersion was transferred to an autoclave for a hydrothermal reaction at 100 °C for 24 hours. Afterward, the temperature of the mixture was reduced to ambient temperature, and the mixture was filtered using a Whatman filter paper ($\Phi = 110$ mm). The product was

Open Access Article. Published on 05 June 2017. Downloaded on 9/15/2024 10:19:27 AM.
This article is licensed under a Creative Commons Attribution-NonCommercial 3.0 Unported Licence.

washed with distilled water 3 times and 95% ethanol twice. After drying under vacuum at 105 °C for 24 h, the achieved powder was calcined at room temperature to 550 °C for 8 hours followed by heating at 550 °C for 6 hours.

With the catalytic base (pH = 9.5–10), the hydrolysis reaction of TEOS easily forms $Si(OH)_4$ with OH^- ions that can directly penetrate toward the Si atoms and replace every part of the $-OC_2H_5$ group in the TEOS molecule. Therefore, condensing the ≡Si(OH) group of silica gel made up with structural hierarchical priorities for all sides, resulting in nanosilica material that often formed spherical sructures.[23,33–38] The preparation procedure is shown in Scheme 1.

2.3 Characterization

X-ray diffraction (XRD, Shimadzu XD-D1) was used to determine the crystallinity with monochromatic high-intensity CuKα radiation (λ = 1.5406 Å). The shape and structure of the nanomaterial surface was analyzed at a high-resolution using SEM (JSM-5600 JEOL, Japan). UV-vis diffuse reflectance spectra (DRS) analysis was conducted using a UV-vis spectrophotometer (Neosys-2000) by using $BaSO_4$ as reference at room temperature and converted from reflection to absorbance by the Kubelka–Munk method. Transmission electron microscopy (TEM) was also used to examine the size and distribution of the titanium and iron particles deposited on the fullerene surface of various samples. High Resolution Transmission Electron Microscopy (HRTEM, JEOL, JEM-2010, Japan) was used to observe the surface state and structure of the survey composites at an acceleration voltage of 200 kV. The TEM specimens were prepared by placing a few drops of sample solution on a carbon grid. The XPS analysis was performed using a VG Scientific ESCALAB250 XPS system equipped with a monochromated Al Kα X-ray source ($h\nu$ = 1486.6 eV) with charge compensation. The Raman spectra of the prepared samples was observed using a spectrometer (Jasco Model Name NRS-3100) with an excitation laser wavelength of 532.06 nm. Nitrogen adsorption/desorption isotherms studies were prepared using a Micromeritics ASAP 2020M + C operating at 77 K using the Brunauer–Emmett–Teller (BET) method to determine the surface area. The survey samples were degassed at 150 °C for 4 h prior to the surface area measurements, whereas the pore size distribution was calculated according to the Barret–Joyner–Halenda (BJH) method. Photoelectrochemical measurements were performed using a self-made photoelectrochemical system installed a 250 W halogen lamp as the irradiation source. The photocurrent measurement was performed by a computer-controlled VersaSTAT-3 electrochemical analyzer. A survey composite modified photoelectrode with an active area of 1 cm^2 was used as the working electrode, and a Pt wire and saturated Ag/AgCl were used as the counter and reference electrodes, respectively. All the photocurrent measurements were conducted by dipping the survey composite modified photoelectrode into a mixture of 0.1 M KCl and 0.5 M TEA at a constant potential of 0 V *vs.* Ag/AgCl. A UV/Vis spectrophotometer (Optizen POP, Mecasys, Korea) was used for the photodegradation experiments.

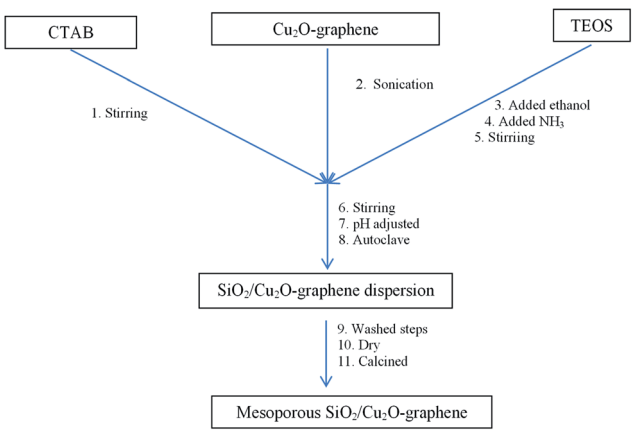

Scheme 1 Synthesis of mesoporous SiO_2/Cu_2O–graphene by a simple self-assembly method.

2.4 Photocatalytic activity

For the typical photocatalytic test carried out at room temperature, the mesoporous SiO_2/Cu_2O–graphene nanocomposite used in this study was found to be 0.05 g, dissolved in 100 mL RhB solution (200 ppm). Prior to the irradiation, the above mixture solution was maintained in a dark box for 2 hours to establish the adsorption/desorption equilibrium of organic dyes. Next, the solution was irradiated with visible light radiation (λ ≥ 420 nm). The first sample was withdrawn at the end of the dark adsorption period before switching on the light to determine the RhB concentration in the solution after dark adsorption. The starting point ($t = 0$) of the reaction was defined as the point where the concentration of RhB solution was recorded as c_0. Afterward, these samples were extracted from the solution mixtures in the reactor at regular intervals of 30, 60, 90, 120, and 180 min. The powders were dispersed using a centrifuge machine (10 000 ppm/15 min) before the analysis. The dye concentration in the solution was measured as a function of the irradiation time. The photodegradation of the MB and RBB solution proceeded following a similar process.

A UV-spectrophotometer (Opizen POP, Korea) was used to analyze the photodegradation of the dye solutions in terms of the concentration (c). A spectrophotometric analysis was performed on each sample of the dye solutions at regular time intervals to obtain the absorbance spectrum. The spectral range was investigated at λ_{max} = 554 nm, 665 nm, 591 nm, respectively, for RhB, MB, and RBB by using a calibration curve since no reaction occurred with the absorption of products at these wavelengths. The degradation capacity (η%) was calculated as

$$\eta(\%) = (1 - c/c_0) \times 100$$

The photodegradation of organic dyes was also observed for RhB, MB, and RBB with (a) Cu_2O–graphene, (b) Cu_2O–graphene–TiO_2, (c) mesoporous SiO_2/Cu_2O–graphene and (d) Cu_2O particles, following the same procedure as that mentioned above.

 This journal is © The Royal Society of Chemistry 2017

Open Access Article. Published on 05 June 2017. Downloaded on 9/15/2024 10:19:27 AM.
This article is licensed under a Creative Commons Attribution-NonCommercial 3.0 Unported Licence.

Next, recycling experiments were carried out for five repeated cycles to investigate the stability of the photocatalytic performance. After each cycle, the catalyst was centrifuged, washed with ethanol, deionised water, and dried before reuse for the next experiment.

3. Results and discussion

3.1 Characterization

An X-ray diffraction (XRD) analysis was conducted with the composites to obtain the component crystalline phase information and assess the purity and crystalline size of the nanocomposite. The XRD results of the mesoporous SiO_2/Cu_2O–graphene calcined at 550 °C is shown in Fig. 1. All diffraction peaks were clear, and the purity of the mesoporous SiO_2/Cu_2O–graphene was expressed through the presence of two types of main diffraction peaks with Cu_2O and SiO_2 signals, without any unexpected peaks. Because of the dominant effect of silica, the presence of SiO_2 particles is seen through the broad diffraction peak at 2θ of 22.96°.[39,40] Next, according to the XRD results shown in Fig. 1, the Cu_2O signal was confirmed by the clear distribution of the peaks obtained according to the Miller index planes corresponding to (110), (111), (200), (220) and (311) (JCDS 78-2076), respectively.[41,42] On the other hand, no graphene peaks were recorded in the XRD patterns of the nanocomposites, indicating that the immobilization of SiO_2 particles onto the surface of the graphene sheets disturbs the ordered structure of most graphene sheets.[43,44] Looking over Fig. 1, the obtained composites were almost perfect with a single phase, high crystallinity, and high purity due to the absence of unexpected peaks and sharper diffraction peaks. The signal of these single peaks in mesoporous SiO_2/Cu_2O–graphene confirms the development of Cu_2O and SiO_2 on the graphene sheets.

The morphology of the mesoporous SiO_2/Cu_2O–graphene sample was also assessed during the initial evaluation *via* SEM, and the results are presented in Fig. S1 (ESI†). The SEM images also indicate that both fine Cu_2O and SiO_2 nanoparticles uniformly covered the graphene surface. The morphological features of the SiO_2 particles included a small size with spherical shapes and good particle dispersion. This indicates an increased photocatalytic activity with the mesoporous SiO_2/Cu_2O–graphene nanocomposite. With this morphogenesis and sustainable link, the ability to switch the charge between Cu_2O and SiO_2 as well as switch the charge among Cu_2O, SiO_2, and graphene increased. Subsequently, an increased photocatalytic activity with the mesoporous SiO_2/Cu_2O–graphene nanocomposite can be observed.

TEM images were taken for the mesoporous SiO_2/Cu_2O–graphene nanocomposites to further investigate the structure and provide clear images of the dispersion and morphology, as shown in Fig. 2. Fig. 2(a) shows the existence of quantum dots with an irregular shape, which indicates that the Cu_2O nanoparticles covered the surface of the graphene sheets. In Fig. 2(b), smaller Cu_2O nanoparticles with a size around 5–10 ppm can be seen to be uniformly distributed throughout the surface of the small TiO_2 rods with an average size of about 150–200 nm, as well as on the graphene surface. The typical morphologies of the mesoporous SiO_2/Cu_2O–graphene nanomaterials were confirmed in Fig. 2(c and d). It was clear that the spherical silica nanoparticles with a pore diameter smaller than 2 μm were successfully hanged on the graphene surface. In this case, the graphene nanosheets play a major role in a facile template for the TEOS hydrolysis.[37] The results of HR-TEM in Fig. 2(e and f) show the detailed structure of the mesoporous SiO_2/Cu_2O–graphene nanomaterials. Besides the amorphous in nature of the silica particles were clearly seen, the single-crystallinity of Cu_2O nanoparticles were found to exist on the spherical shapes surface of the mesoporous SiO_2 with the pure black microsphere-like shape which implied that the particles is solid and not core–shell or inner hollow structure.[45] The formation of the mesoporous SiO_2 and Cu_2O nanoparticles on the graphene surface was also observed in Fig. 2(f). As a result, the moving charge from SiO_2 to Cu_2O will easily occur and help limit the recombination of the photogenerated electron–holes, releasing the necessary energy for the photodegradation reaction. The mesoporous silica nanoparticles were also promised to provide a more exposed surface for the photocatalytic activity. The above results indicate that the mesoporous SiO_2/Cu_2O–graphene nanomaterial will become a potential candidate due to its photocatalytic activity. The TEM results matched the results from SEM, confirming that the experimental conditions and processes were adequate.

The Raman spectra were measured to consolidate the structural information of the mesoporous SiO_2/Cu_2O–graphene nanocomposite. The Raman spectra of Cu_2O–graphene and mesoporous SiO_2/Cu_2O–graphene nanocomposites were presented in Fig. 3. The existence of the D and G bands in the Raman results is evidence of the presence of carbon in the survey nanomaterials. The D and G bands of the Cu_2O–graphene composite appeared at 1340 cm^{-1} and 1590 cm^{-1}, respectively, while the D band at 1350 cm^{-1} and G band at 1600 cm^{-1} of the mesoporous SiO_2/Cu_2O–graphene nanocomposite was confirmed, as shown in Fig. 3. The D band shifted from

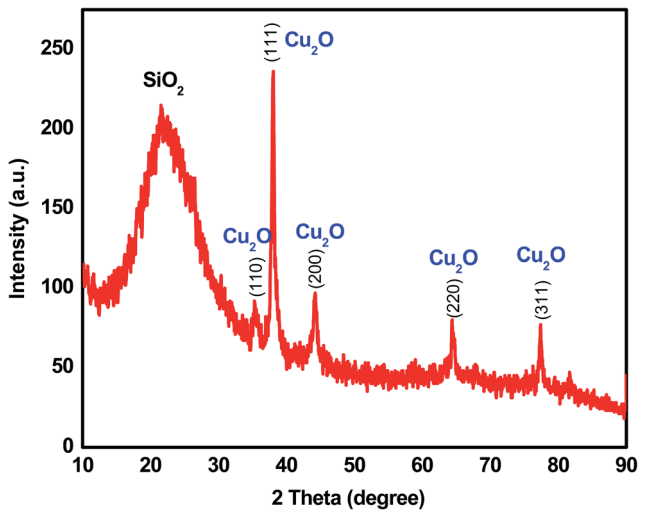

Fig. 1 XRD patterns of the mesoporous SiO_2/Cu_2O–graphene composite.

Open Access Article. Published on 05 June 2017. Downloaded on 9/15/2024 10:19:27 AM.
This article is licensed under a Creative Commons Attribution-NonCommercial 3.0 Unported Licence.

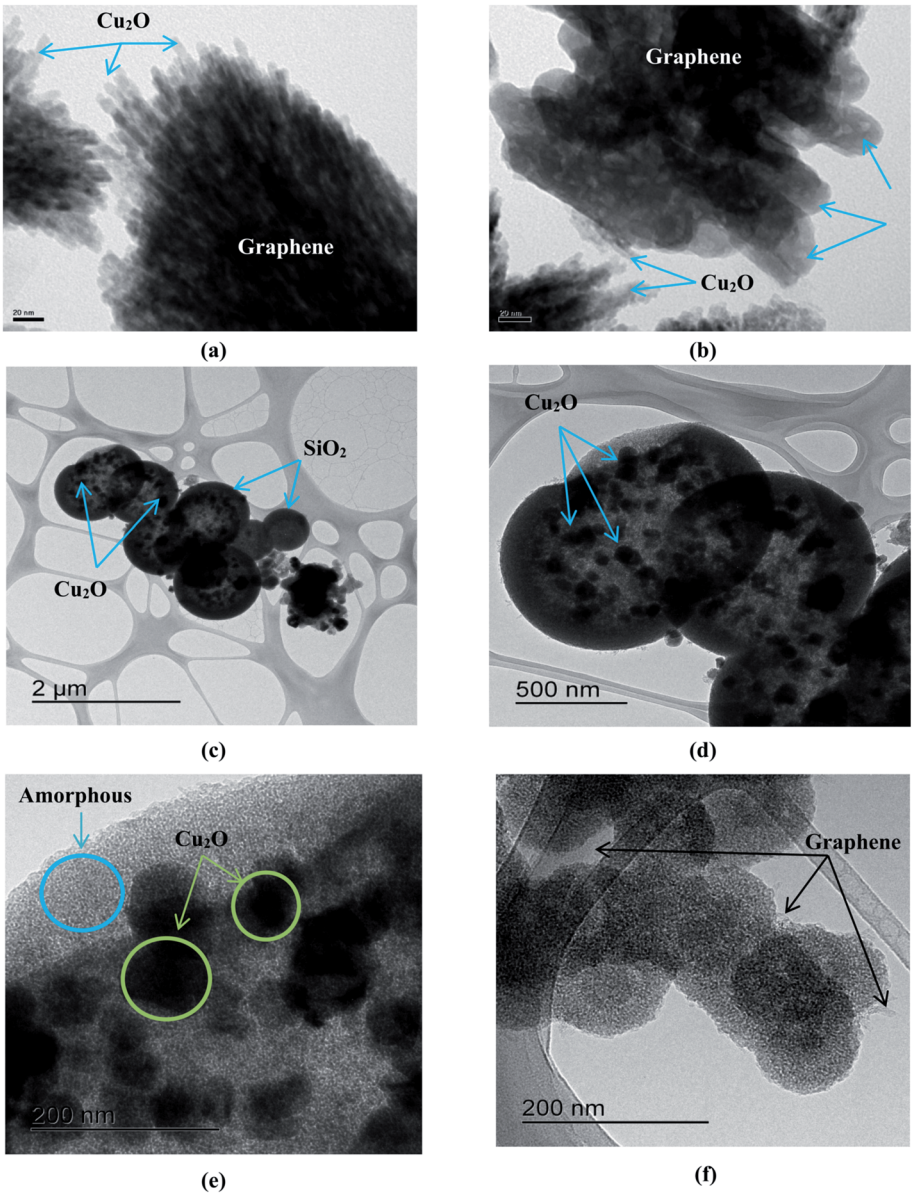

Fig. 2 TEM image of the Cu_2O–graphene (a), Cu_2O–graphene–TiO_2 (b) and mesoporous SiO_2/Cu_2O–graphene (c and d) composites and HR-TEM image of mesoporous SiO_2/Cu_2O–graphene (e and f).

1340 to 1350 cm^{-1}, indicating changes in the chemical bond between Cu_2O–graphene and mesoporous SiO_2/Cu_2O–graphene nanocomposite. In the graphene oxide-based samples, the D band is an ordinary feature of sp^3 defects, and the G band provides information on the in-plane vibration of the sp^2 bonded carbons.[46] The intensity ratio (I_D/I_G) reflects the order of defects in the graphene oxide or graphene. It strongly depends on the extent of the disorder in the graphitic material.[47] Following Fig. 3, the calculated I_D/I_G ratio of the Cu_2O–graphene composite was found to be 0.960, while the I_D/I_G ratio of mesoporous SiO_2/Cu_2O–graphene was 0.897. The decrease in the I_D/I_G ratio indicates an increase in the number of graphene layers or a partial reduction in the graphene oxide into graphene, which is consistent with the reports.[48] In other words, the decrease in I_D/I_G proved that sp^2 carbon domains were repaired, but a certain amount of sp^3 or twisted carbon atoms as defects still existed.[49] Furthermore, the lower I_D/I_G ratio shows a better defect repair mechanism.[50]

The typical FT-IR spectrum of the survey materials was taken as shown in Fig. 4(a). Considering the FT-IR spectrum of the Cu_2O–graphene nanocomposites, it shows three main peaks that can be attributed to oxygen-containing groups. The peaks centered at 1110, 1400, and 1560 cm^{-1} assisted the C–O vibrations from the alkoxy groups, C–OH stretching vibrations, and C=O stretching peak of the conjugated ketone, respectively.[51,52] After a self-assembly reaction with TEOS at pH 9.5–10, the FI-IR spectrum of mesoporous SiO_2/Cu_2O–graphene nanocomposite displayed new bands, confirming that the silica nanoparticles covered the graphene surface. The bands at 805 and 1080 cm^{-1} were attributed to Si–O–Si symmetric stretching, and the

 This journal is © The Royal Society of Chemistry 2017

Open Access Article. Published on 05 June 2017. Downloaded on 9/15/2024 10:19:27 AM.
This article is licensed under a Creative Commons Attribution-NonCommercial 3.0 Unported Licence.

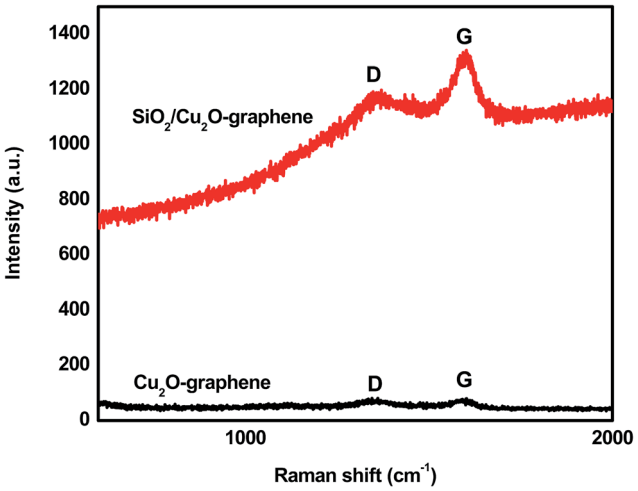

Fig. 3 Raman spectra of the mesoporous SiO_2/Cu_2O–graphene and Cu_2O–graphene nanocomposites.

stretching vibration of the Si–O–Si band, respectively.[53] In contrast with the disappearance of the C=O groups, the above evidence suggests that the typical carboxyl group was altered into Si–O–C bonds.[37] When compared to the FT-IR spectrum of the Cu_2O–graphene nanocomposite between 1300 and 1600 cm^{-1}, it was easy to see the absence of the characteristic peaks for oxygen-containing groups, which indicated that the oxygen-containing groups were unfixed.[39] In other words, all FT-IR spectrum results concluded that mesoporous SiO_2 were produced on the surface of the graphene sheets. As the XPS results show in Fig. 4(b and c), the surface bonding state of the survey nanomaterial was identified as containing Si included Si 2p, and Si 2s at 106 eV, and 155 eV, respectively. The C 1s spectra of the composites were presented in the region from 282.5–294.7 eV, indicating the presence of non-oxygenated C (C=C/C–C) in aromatic rings (284.5 eV), as well as the C in C–O–C (286.3 eV), where the epoxy or hydroxyl group (C–O) is at 286.7 eV and C=O or the carboxyl is at 288.1 eV.[54,55] The presence of the O 1s signal of the nanocomposites is due to absorbed oxygen.

The results of the Kubelka–Munk transformation from the UV-vis diffuse reflectance spectra of the mesoporous SiO_2/Cu_2O–graphene composite are displayed in Fig. 5. The band gap energy value was achieved at the point at which the straight line approaching the curve intersects the horizontal axis. The band gap energy values of the mesoporous SiO_2/Cu_2O–graphene composite correspond to 1.80 eV, which is lower than that of the Cu_2O–graphene composite.[56] This phenomenon promises an increase in the catalytic activity of the mesoporous SiO_2/Cu_2O–graphene composite.

The surface properties and the results of the porosity analysis of the composites are exhibited in Fig. 6, and the corresponding textural parameters are displayed in Table 1. The nitrogen adsorption/desorption isotherm results of the Cu_2O–graphene, Cu_2O–graphene–TiO_2 composites clearly exhibit a similar type II curve. The pore size calculated using the BJH method was about 24.15 and 11.29 nm. The BET surface area of the Cu_2O–graphene and Cu_2O–graphene–TiO_2 composites was

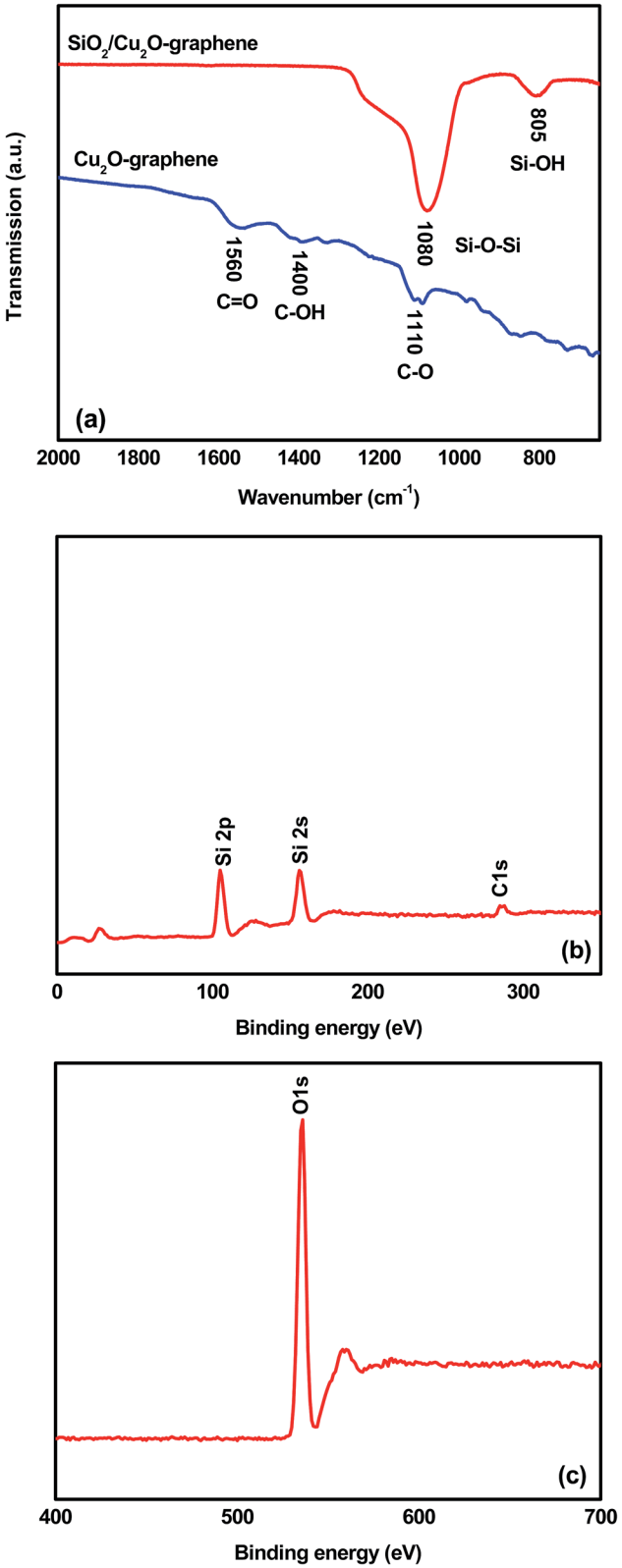

Fig. 4 FT-IR spectra of the Cu_2O–graphene and mesoporous SiO_2/Cu_2O–graphene composites and XPS results of the mesoporous SiO_2/Cu_2O–graphene composites.

Open Access Article. Published on 05 June 2017. Downloaded on 9/15/2024 10:19:27 AM.
This article is licensed under a Creative Commons Attribution-NonCommercial 3.0 Unported Licence.

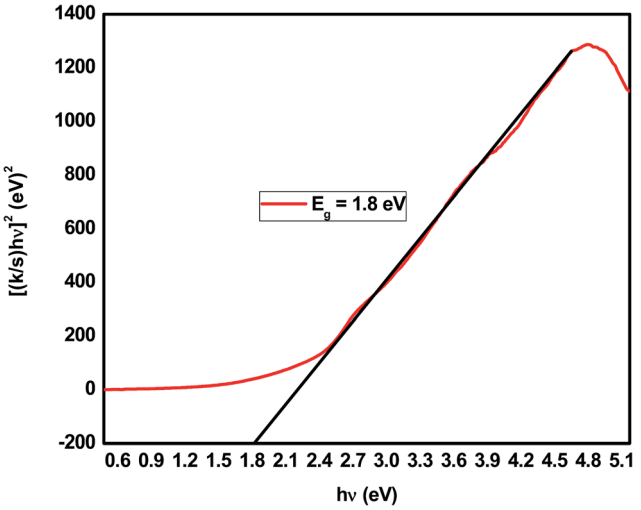

Fig. 5 $h\nu$ *versus* $[(k/s)h\nu]^2$ graph of the mesoporous SiO_2/Cu_2O–graphene composite.

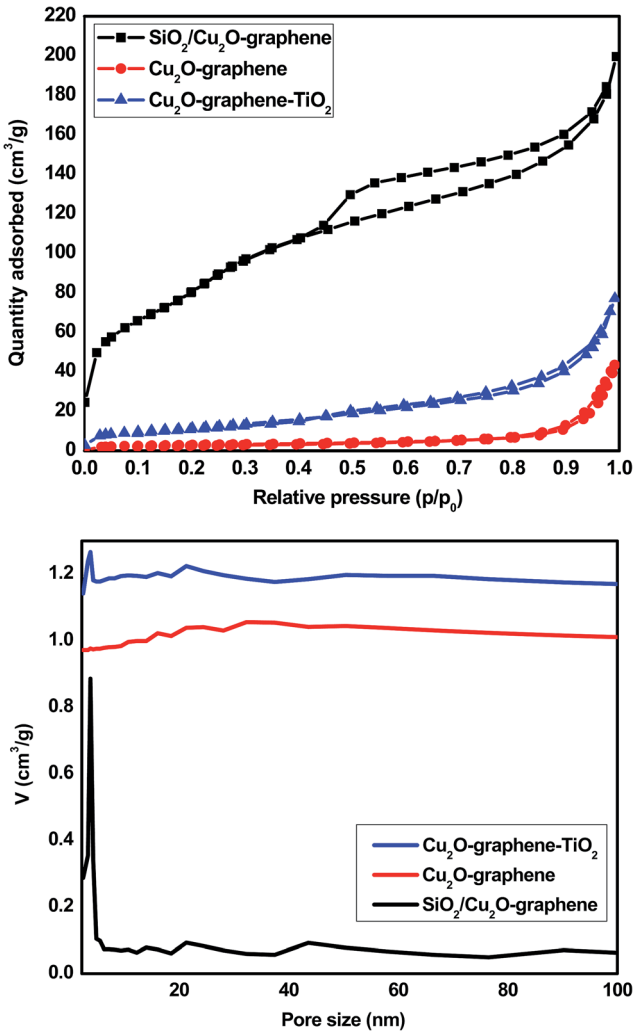

Fig. 6 The nitrogen adsorption/desorption isotherms (above) and pore size distributions (below) for the Cu_2O–graphene, Cu_2O–graphene–TiO_2 and mesoporous SiO_2/Cu_2O–graphene composites.

Table 1 Micropore structure parameters of the Cu_2O–graphene, Cu_2O–graphene–TiO_2 and mesoporous SiO_2/Cu_2O–graphene composites

Sample name	BET (m^2 g^{-1})	Total pore volume (cm^3 (STP) g^{-1})	Average pore size (nm)
Cu_2O–graphene	10.74	2.47	24.15
Cu_2O–graphene–TiO_2	41.55	9.55	11.29
SiO_2/Cu_2O–graphene	287.49	66.05	4.19

10.74 and 41.55 m^2 g^{-1}, respectively. According to the hysteresis loop in the relative pressure region around 0.45–0.98, the nitrogen adsorption/desorption isotherms showed that the SiO_2/Cu_2O–graphene nanocomposite exhibited a similar type IV curve. In other words, the SiO_2/Cu_2O–graphene nanocomposite existed with a mesoporous structure. After the self-assembly method with TEOS, the surface area of the SiO_2/Cu_2O–graphene inhibited a big difference in the Cu_2O–graphene, Cu_2O–graphene–TiO_2 composites. Due to the mesoporous structure, the SiO_2/Cu_2O–graphene showed a nanopore size of 4.19 nm and a very large surface area with BET results at about 287.49 m^2 g^{-1}. Besides, the total pore volume of SiO_2/Cu_2O–graphene was 66.05 cm^3 g^{-1}, which is 33 times more than the total pore volume of Cu_2O–graphene (2.47 cm^3 g^{-1}). With an increase in the surface area and decrease in the pore size, as well as the large total pore volume, the SiO_2/Cu_2O–graphene is expected to have a high photocatalytic activity.

Fig. 7 displays the photocurrent response of the ITO/as-prepared nanocomposites based on time under visible light irradiation, which was carried out for five times at 20 s intervals. It was obviously observed that no current was observed in the dark, which provides the evidence of no photoinduced charge separation occurs. The as-synthesized Cu_2O–graphene presented the high photocurrent response (~98.0 μA cm^{-2}) during repeating on–off illumination cycles, while the low photocurrent density was ~20.0 μA cm^{-2} for SiO_2–graphene nanocomposite. Besides, the mesoporous SiO_2 and Cu_2O–graphene combination with a mass ratio at 100 : 5 reached two times enhanced photocurrent density (~40.0 μA cm^{-2}) compared to SiO_2–graphene nanocomposite. The improved photocurrent of the mesoporous SiO_2/Cu_2O–graphene implied an enhanced the

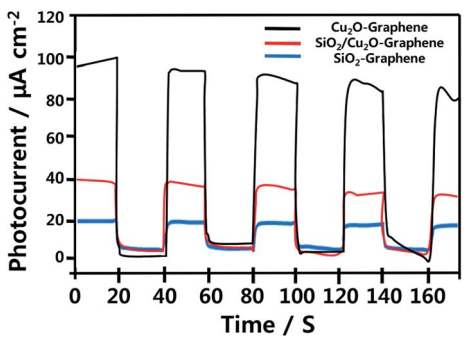

Fig. 7 Photocurrent measurement with Cu_2O–graphene, mesoporous SiO_2/Cu_2O–graphene and SiO_2–graphene modified photoelectrodes.

This journal is © The Royal Society of Chemistry 2017

Open Access Article. Published on 05 June 2017. Downloaded on 9/15/2024 10:19:27 AM.
This article is licensed under a Creative Commons Attribution-NonCommercial 3.0 Unported Licence.

photoinduced electron–hole separation at the p–n junction of the SiO_2/Cu_2O hybrid, while the holes were scavenged by the TEA, and graphene plays a role as a charge transfer medium.[57,58] As the results, the electrons were transported to the ITO electrode, resulting in photocurrent generation. Because of the reduced interaction between as-prepared survey nanocomposites and ITO under visible light irradiation, the photocurrent density decreased over time.[59] On the other hand, the porous network structure also contributes to the enhanced transition of photogenerated carriers.[60]

3.2 Photodegradation

The organic dye degradation progressed in two stages. First, the adsorption/desorption equilibrium of organic dyes was established in a dark box for 2 hours. Then, the photocatalytic degradation experiment of the dye solutions was conducted under visible light irradiation with different irradiation times (from 0 to 180 min). The effects of the different organic dyes are given below.

3.2.1 Degradation of rhodamine B (RhB). Fig. 8 shows the photocatalytic degradation of the RhB aqueous solution in the present of the Cu_2O–graphene, Cu_2O–graphene–TiO_2, mesoporous SiO_2/Cu_2O–graphene composites and Cu_2O at room temperature. As shown in Fig. 8, in the RhB case, the adsorption effect of the mesoporous SiO_2/Cu_2O–graphene was maximized. A longer time resulted in a decrease in the maxima of the absorption intensity in the visible region (around 555 nm). The mesoporous SiO_2/Cu_2O–graphene nanocomposite expressed the best photodegradation, with a value of around 89.27%, which is a big difference when compared to that of Cu_2O–graphene–TiO_2 (41.26%). The most significant difference in the photocatalytic effect of the Cu_2O–graphene (9.50%) and Cu_2O (4.35%) compared to the mesoporous SiO_2/Cu_2O–graphene can also be seen. We noticed that the mesoporous SiO_2/Cu_2O–graphene composite provided the best degradation for the RhB solution.

3.2.2 Degradation of methylene blue (MB). The results of the photodegradation of the survey composites with MB were investigated under the same experimental conditions shown in Fig. 9. The MB case also showed that the adsorption effect of the mesoporous SiO_2/Cu_2O–graphene is better than that of the Cu_2O–graphene, Cu_2O–graphene–TiO_2, and Cu_2O after being maintained for 2 hours in the dark. The effect of the photodegradation on mesoporous SiO_2/Cu_2O–graphene far exceeds that of both Cu_2O–graphene, Cu_2O–graphene–TiO_2, and Cu_2O with 68.62, 12.08%, 12.46%, and 3.63% respectively.

3.2.3 Degradation of reactive black B (RBB). Fig. 10 shows the degradation results of the Cu_2O–graphene, Cu_2O–graphene–TiO_2 and mesoporous SiO_2/Cu_2O–graphene composites and Cu_2O under visible light irradiation with the RBB solution. The results shown in Fig. 10 indicate that the degradation efficiency decreased as the irradiation time increased. All survey composites achieved a 60% removal for the RBB solution. After 180 min under visible light irradiation, the mesoporous SiO_2/Cu_2O–graphene retained the highest photodegradation effect of 84.07%. Meanwhile, the photodegradation results for Cu_2O–graphene, Cu_2O–graphene–TiO_2, and Cu_2O were 67.98%, 74.51%, and 10.94% respectively. The above results indicate that the mesoporous SiO_2/Cu_2O–graphene has potential as a material with high photodegradation activity.

Photocatalytic reactions with different photocatalysts can be expressed using the Langmuir–Hinshelwood model.[61] The photocatalytic degradation of organic dyes containing different photocatalysts obeys pseudo-first-order kinetics with respect to the concentration of the organic dyes.

$$-dc/dt = k_{app}c \quad (I)$$

The integration of (I) (with the restriction of $c = c_0$ at $t = 0$, with c_0 as the initial concentration in the bulk solution after

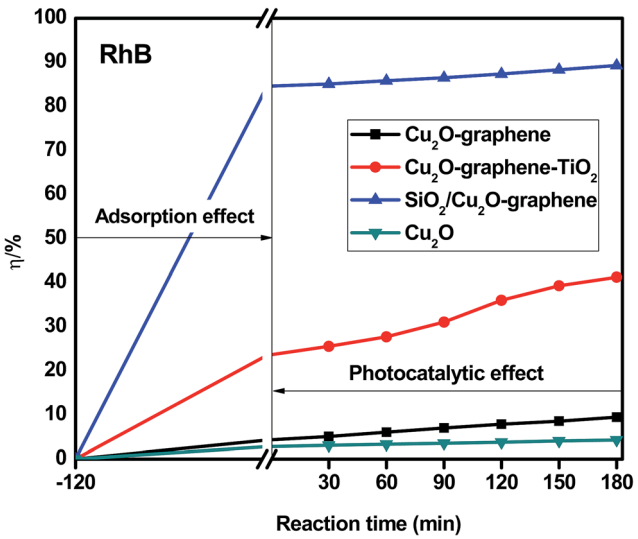

Fig. 8 Degradation efficiency of different composites with RhB under visible light. The concentration of RhB was 200 ppm. The amount of composites were 0.05 g.

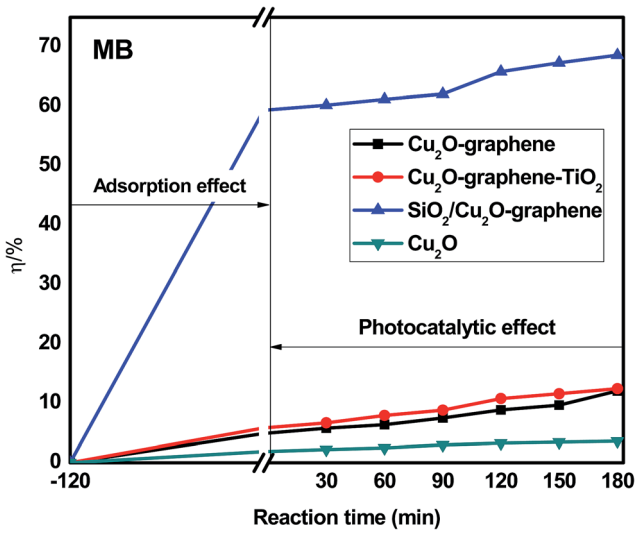

Fig. 9 Degradation efficiency of different composites with MB under visible light. The concentration of MB was 200 ppm. The amount of composites were 0.05 g.

Open Access Article. Published on 05 June 2017. Downloaded on 9/15/2024 10:19:27 AM.
This article is licensed under a Creative Commons Attribution-NonCommercial 3.0 Unported Licence.

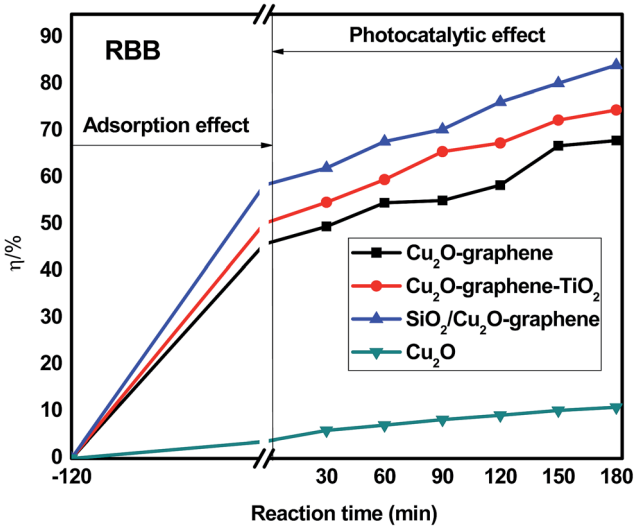

Fig. 10 Degradation efficiency of different composites with RBB under visible light. The concentration of RBB was 200 ppm. The amount of composites were 0.05 g.

dark adsorption and t the reaction time) will lead to the following expected relation:

$$-\ln(c/c_0) = k_{app}t \quad \text{(II)}$$

where c and c_0 are the reactant concentration at time $t = t$ and $t = 0$, respectively, k_{app} and t are the apparent reaction rate constant and time, respectively. According to (II), a plot of $-\ln(c/c_0)$ *versus* t will yield a slope of k_{app}. The results are shown in Fig. S2 (ESI†).

To investigate the stability of the photocatalytic performance, the mesoporous SiO_2/Cu_2O–graphene was used to degrade the RhB dye in five repeated cycles, and the results are shown in Fig. S3 (ESI†). As shown in Fig. S3(a),† the photocatalytic activity of the mesoporous SiO_2/Cu_2O–graphene still exhibited good results after five recycling runs. This confirmed that the mesoporous SiO_2/Cu_2O–graphene had a high stability under visible light irradiation. In spite of the lower diffraction peak intensity, we can see three types of main diffraction peaks indexed to Cu_2O, and SiO_2 signals still remain in the XRD patterns in Fig. S3(b).† The TEM image from Fig. S3(c)† also presented the original structure of the mesoporous SiO_2/Cu_2O–graphene nanocomposite after five cycling photocatalysis process. Therefore, we can conclude that the mesoporous SiO_2/Cu_2O–graphene composite has the good stability during photocatalysis.

Besides the narrowing of the band gap energy, the excellent photocatalytic activity of the mesoporous SiO_2/Cu_2O–graphene is explained to be a result of the pore diameter, pore volume and surface area. Graphene oxide and silica nanoparticles provided a large surface for photodegradation, and in the photodegradation experiments, we can see that the adsorption capacities of the mesoporous SiO_2/Cu_2O–graphene are higher than those for Cu_2O, Cu_2O–graphene and Cu_2O–graphene–TiO_2 mainly due to the large surface area of the mesoporous silica particles.[62] In our case, the BET of mesoporous SiO_2/Cu_2O–graphene was more than 7–28 times that for the BET results of the Cu_2O–graphene and Cu_2O–graphene–TiO_2 composites. With these outstanding properties, the adsorption effects of mesoporous SiO_2/Cu_2O–graphene produced the best adsorption effects for the RhB, MB, and RBB solution.

Graphene oxide also plays the role of an electron acceptor, photosensitizer, and the adsorbent to efficiently enhance the photodegradation of organic dyes.[63,64] The presence of the high density of oxygen-containing functional groups, such as hydroxyl groups, epoxy, and carboxyl at the edge or on the large surface area of graphene oxide provides the more space for ionic/electro interaction between dye molecules and the aromatic rings of graphene oxide sheets, and from that, the better adsorptivity can be achieved.[65,66] Besides, we can not ignore the role of an electron acceptor of graphene oxide which participates in facilitating electron transfer process from SiO_2 and Cu_2O to join the reduction reaction as well as enhancing charge separation and therefore, enhancing the photodegradation.[67,68]

On the other hand, the mesoporous structure of the silica nanoparticles plays a major role in the increased photodegradation effect as well as the surface of graphene sheets. In this case, the mesoporous structure allows a greater amount of guest species over the catalysts, and the reaction will not be limited to the photocatalytic surface. For the large surface area, the active site population and accessibility to the active sites increase, and the photocatalytic activity will thus increase.[69]

The photocatalytic activity of the mesoporous SiO_2/Cu_2O–graphene composite reflects two factors that influence the degradation rate: the adsorption capacity due to the mesoporous structure and the decomposition effect through catalysis. The valence band of the SiO_2 is higher than that of Cu_2O. Therefore, the photogenerated electrons of SiO_2 can switch to the valence band of Cu_2O and then shift to the graphene surface to join the reduction reaction (e^-_{CB}). The photogenerated holes of Cu_2O can also switch the graphene surface to participate in oxidation reactions (h^+_{VB}). With this mechanism, the reduced electron–hole recombination leads to an increase in the catalytic ability. The photogenerated electron–hole shifts to the surface and interacts with substances, such as the hydroxyl group and oxygen, where the adsorption creates free radicals on the surface of the semiconductor.[70,71]

4. Conclusions

The results of the experiments above indicate that we successfully synthesized mesoporous SiO_2/Cu_2O–graphene composites by combining TEOS and Cu_2O–graphene with CTBA at pH 9.5–10 and calcined at 550 °C. The XRD investigation of the photocatalyst showed the presence of silica nanoparticles due to broad diffraction peaks as well as a cubic Cu_2O phase. SEM and TEM images suggested that both Cu_2O and SiO_2 nanostructures were successfully loaded onto the transparent graphene sheets. Furthermore, the spherical silica nanoparticles with pore diameter as well as the quantum dot-sized Cu_2O are promising materials that can enhance the photocatalytic activity of mesoporous SiO_2/Cu_2O–graphene composites. The Raman and DRS

 This journal is © The Royal Society of Chemistry 2017

Open Access Article. Published on 05 June 2017. Downloaded on 9/15/2024 10:19:27 AM.
This article is licensed under a Creative Commons Attribution-NonCommercial 3.0 Unported Licence.

spectrum also confirm the structures of the mesoporous SiO_2/Cu_2O–graphene composite, and the FT-IR spectrum shows the structural differences between the Cu_2O–graphene and mesoporous SiO_2/Cu_2O–graphene composite through the appearance of a new characteristic band and the removal of oxygen-containing groups. The nitrogen adsorption/desorption isotherm provided information regarding the pore diameter, pore volume, and surface area. The photocurrent analyses also provided the evidence of the enhanced photocatalytic activity of the mesoporous SiO_2/Cu_2O–graphene composite.

The mesoporous structure of the silica nanoparticles plays a major role in increasing the photodegradation effect as well as the surface of the graphene sheets. The results of this study thus show that the material is capable of the photocatalytic degradation of different organic dyes under visible light irradiation. The results of the photodegradation suggest that the mesoporous SiO_2/Cu_2O–graphene composite is much more effective photocatalyst than both Cu_2O–graphene, Cu_2O–graphene–TiO_2 composites and Cu_2O when under the same experimental conditions.

References

1 Y. He, N. Zhang, L. Zhang, Q. Gong, M. Yi, W. Wang, H. Qiu and J. Gao, *Mater. Res. Bull.*, 2014, **51**, 397–401.
2 F. Xu, Y. Yuan, D. Wu, M. Zhao, Z. Gao and K. Jiang, *Mater. Res. Bull.*, 2013, **48**, 2066.
3 Q. Zhou, Y. Zhong, X. Chen, X. J. Huang and Y. C. Wu, *Mater. Res. Bull.*, 2014, **51**, 244.
4 A. Safavi, F. A. Mahyari and M. Tohidi, *Mater. Res. Bull.*, 2013, **48**, 3399.
5 L. Zhu, Z. D. Meng, M. L. Chen, F. J. Zhang, J. G. Choi, J. Y. Park and W. C. Oh, *J. Photocatal. Sci.*, 2010, **1**, 69.
6 H. Zhang, X. Lv, Y. Li, Y. Wang and J. Li, *ACS Nano*, 2010, **4**, 380–386.
7 S. R. Kim, M. K. Parvez and M. Chhowalla, *Chem. Phys. Lett.*, 2009, **483**, 124–127.
8 D. C. T. Nguyen, K.-Y. Cho and W.-C. Oh, *Appl. Surf. Sci.*, 2017, **412**, 252–261.
9 G. Williams, B. Seger and P. V. Kamat, *ACS Nano*, 2008, **2**(7), 1487–1491.
10 J. Li, K. Yu, K. Qian, H. Cao, X. Lu and J. Sun, *Nanoscale Res. Lett.*, 2014, **9**, 172–180.
11 T. Xiong, F. Dong, Y. Zhou, M. Fu and W.-K. Ho, *J. Colloid Interface Sci.*, 2015, **447**, 16–24.
12 Y. Li, Y. Sun, F. Dong and W.-K. Ho, *J. Colloid Interface Sci.*, 2014, **436**, 29–36.
13 P. E. de Jongh, D. Vanmaekkelbergh and J. J. Kelly, *Chem. Commun.*, 1999, 1069–1070.
14 B. Rai, *Sol. Cells*, 1988, **25**, 265–271.
15 M. Hara, T. Kondo, M. Komoda, S. Ikeda, K. Shinohara, A. Tanaka, J. N. Kondo and K. Domen, *Chem. Commun.*, 1998, **3**, 357–358.
16 K. Domen, J. N. Kondo, M. Hara and T. Takata, *Bull. Chem. Soc. Jpn.*, 2000, **73**, 1307–1331.
17 L. Huang, F. Peng, H. Yu and H. J. Wang, *Solid State Sci.*, 2009, **11**, 129–138.
18 Z. Gao, J. Liu, F. Xu, D. Wu, Z. Wu and K. Jiang, *Solid State Sci.*, 2012, **14**, 276–280.
19 C. Kunfeng, L. Jun and X. Dongfeng, *Energy and Environment Focus*, 2012, **1**, 50–67.
20 F. Zhang, Y. Li, Y.-e. Gu, Z. Wang and C. Wang, *Microchim. Acta*, 2011, **173**, 103–109.
21 Y. C. Hsu, Y. T. Hsu, H. Y. Hsu and C. M. Yang, *Chem. Mater.*, 2007, **19**, 1120–1126.
22 M. Tiemann, *Chem. Mater.*, 2008, **20**, 961–971.
23 N. Venkatathri, *Bull. Mater. Sci.*, 2007, **30**, 615–617.
24 Y. J. Acosta-Silva, R. Nava, V. Hernández-Morales, S. A. Macías-Sánchez, M. L. Gómez-Herrera and B. Pawelec, *Appl. Catal., B*, 2011, **110**, 108–117.
25 T. Kamegawa, D. Yamahana and H. Yamashita, *J. Phys. Chem. C*, 2010, **114**, 15049–15053.
26 H. T. Phuong, D. T. Ngo, N. D. Toan, T. T. Son, N. T. Ngoc Bich, N. H. Anh, N. L. Anh and P. H. Trang, *Petrovietnam*, 2016, **9**, 24–33.
27 H. Song, L. Zhang, C. He, Y. Qu, Y. Tian and Y. Lv, *J. Mater. Chem.*, 2011, **21**, 5972–5977.
28 Z. Y. Wang, Q. F. Lu, M. G. Kong and L. D. Zhang, *Chem.–Eur. J.*, 2007, **13**, 1463–1670.
29 Y. Li, X. L. Zhang, R. Qiu, R. Qiao and Y. S. Kang, *J. Phys. Chem. C*, 2007, **111**, 10747–10750.
30 P. Poizot, S. Laruelle, S. Grugeon, L. Dupont and J. M. Tarascon, *Nature*, 2000, **407**, 496–499.
31 Y. Mao, T. Park, F. Zhang and H. Zhou, *Small*, 2007, **7**, 1122–1139.
32 Z. Wang, Y. Du, F. Zhang, Z. Zheng, X. Zhang, Q. Feng and C. Wang, *Mater. Chem. Phys.*, 2013, **140**, 373–381.
33 S. Giri, *Synthesis and characterization of zirconia coated silica nanoparticles for catalytic reactions*, National Institute of Technology, Rourkela, India, 2008.
34 J. Knipping, H. Wiggers, B. Rellinghaus, P. Roth, D. Konjhodzic and C. Meier, *J. Nanosci. Nanotechnol.*, 2004, **4**(8), 1039–1044.
35 L. Hao, X. Gong, S. Xuan, H. Zhang, X. Gong, W. Jiang and Z. Chen, *Appl. Surf. Sci.*, 2006, **252**(24), 8724–8733.
36 T. Sugama and B. Lipford, *J. Mater. Sci.*, 1997, **32**(13), 3523–3534.
37 Q. Sun, P. J. Kooyman, J. G. Grossmann, P. H. H. Bomans, P. M. Frederik, P. C. M. M. Magusin, T. P. M. Beelen, R. A. Van Santen and N. A. J. M. Sommerdijk, *Adv. Mater.*, 2006, **15**(13), 1097–1100.
38 S. H. Zhang, I. Laurer and K. K. Unger, *Adv. Mater.*, 1997, **9**, 254.
39 X. M. Guo, X. G. Liu, B. S. Xu and T. Dou, *Colloids Surf., A*, 2009, **345**, 141–146.
40 W. L. Zhang and H. J. Choi, *Langmuir*, 2012, **28**(17), 7055–7062.
41 Joint Committee on Powder Diffraction Standards, Diffraction Data File, No. 5–666, ICDD International Center for Diffraction Data (formerly JCPDS), Pennsylvania, USA, 1991.
42 F. Zhang, Y. Li, Y.-e Gu, Z. Wang and C. Wang, *Microchim. Acta*, 2011, **173**, 103–109.

Open Access Article. Published on 05 June 2017. Downloaded on 9/15/2024 10:19:27 AM.
This article is licensed under a Creative Commons Attribution-NonCommercial 3.0 Unported Licence.

43 Q. Liu, J. B. Shi, T. Wang, L. X. Zeng and G. B. Jiang, *Angew. Chem., Int. Ed.*, 2011, **50**, 5913–5917.
44 X. Zhou and T. Shi, *Appl. Surf. Sci.*, 2012, **259**, 566–573.
45 L. Chen, Y. Zhang, P. Zhu, F. Zhou, W. Zeng, D. D. Lu, R. Sun and C. Wong, *Sci. Rep.*, 2015, **5**, 9672.
46 J. Zhang, Z. Xiong and X. S. Zhao, *J. Mater. Chem.*, 2011, **21**, 3634–3640.
47 J. Shen, B. Yan, M. Shi, H. Ma, N. Li and M. Ye, *J. Mater. Chem.*, 2011, **21**, 3415–3421.
48 K. Kudin, B. Ozbas, H. Schniepp, R. Prud'homme, I. Aksay and R. Car, *Nano Lett.*, 2008, **8**, 36.
49 X. Zhou and T. Shi, *Appl. Surf. Sci.*, 2012, **259**, 566–573.
50 K. Ullah, S. Ye, S. B. Jo, L. Zhu, K. Y. Cho and W. C. Oh, *Ultrason. Sonochem.*, 2014, **21**(5), 1849–1857.
51 S. J. Park, J. H. An, R. D. Piner, I. Jung, D. X. Yang, A. Velamakanni, S. B. T. Nguyen and R. S. Ruoff, *Chem. Mater.*, 2008, **20**, 6592–6594.
52 A. V. Murugan, T. Muraliganth and A. Manthiram, *Chem. Mater.*, 2009, **21**, 5004–5006.
53 W. G. Leng, M. Chen, S. X. Zhou and L. M. Wu, *Langmuir*, 2010, **26**, 14271–14275.
54 Y. Qi, J. R. Eskelsen, U. Mazur and K. W. Hipps, *Langmuir*, 2012, **28**, 3489–3493.
55 Y.-W. Hsu, T.-K. Hsu, C.-L. Sun, Y.-T. Nien, N.-W. Pu and M.-D. Ger, *Electrochim. Acta*, 2012, **82**, 152–157.
56 A. A. Dubale, W.-N. Su, A. G. Tamirat, C.-J. Pan, B. A. Aragaw, H.-M. Chen, C.-H. Chen and B.-J. Hwang, *J. Mater. Chem. A.*, 2014, **2**, 18383–18397.
57 Y. Wu, D. Chu, P. Yang, Y. Du and C. Lu, *Catal. Sci. Technol.*, 2015, **5**, 3375–3382.
58 A. Ali and W. C. Oh, *Sci. Rep.*, 2017, **7**(1), 1867.
59 Q. Hao, X. Niu, C. Nie, S. Hao, J. Ge, W. Zou, D. chen and W. Yao, *Phys. Chem. Chem. Phys.*, 2016, **18**, 31410–31418.
60 M. Zhang, W. Luo, Z. Wei, W. Jiang, D. Liu and Y. Zhu, *Appl. Catal., B*, 2016, **194**, 105–110.
61 Y. Li, X. Li and J. Li, *Water Res.*, 2006, **40**, 1119.
62 T. Jiang, A. S. Poyraz, A. Iyer, Y. Zhang, Z. Luo, W. Zhong, R. Miao, A. M. El-Sawy, C. J. Guild, Y. Sun, D. A. Kriz and S. L. Suib, *J. Phys. Chem. C*, 2015, **119**(19), 10454–10468.
63 F. Dong, Z. Y. Wang, Y. J. Sun, W. K. Ho and H. D. Zhang, *J. Colloid Interface Sci.*, 2013, **401**, 70–79.
64 T.-D. Nguyen-Phan, V. H. Pham, E. W. Shin, H.-D. Pham, S. Kim, J. S. Chung, E. J. Kim and S. H. Hur, *Chem. Eng. J.*, 2011, **170**, 226–232.
65 G. Williams, B. Seger and P. V. Kamat, *ACS Nano*, 2008, **2**, 1487–1491.
66 I. V. Lightcap, T. H. Kosel and P. V. Kamat, *Nano Lett.*, 2010, **10**, 577–583.
67 S. Min and G. Lu, *J. Phys. Chem. C*, 2012, **116**(48), 25415–25424.
68 Y. J. Sun, W. D. Zhang, T. Xiong, Z. W. Zhao, F. Dong, R. Q. Wang and W. K. Ho, *J. Colloid Interface Sci.*, 2014, **418**, 317–323.
69 K. Li, T. Chen, L. Yan, Y. Dai, Z. Huang, J. Xiong, D. Song, Y. Lv and Z. Zeng, *Colloids Surf., A*, 2013, **422**, 90–99.
70 R. Raghav, P. Aggarwal and S. Srivastava, *AIP Conf. Proc.*, 2016, **1724**, 020078.
71 J. P. Espinós, J. Morales, A. Barranco, A. Caballero, J. P. Holgado and A. R. González-Elipe, *J. Phys. Chem. B*, 2002, **106**, 6921–6929.

This journal is © The Royal Society of Chemistry 2017